Journal of Magnetic Resonance **144,** 115–122 (2000)
doi:10.1006/jmre.2000.2047, available online at http://www.idealibrary.com on IDEAL®

Electron Spin–Lattice Relaxation Rates for High-Spin Fe(III) Complexes in Glassy Solvents at Temperatures between 6 and 298 K

Yi Zhou, Bruce E. Bowler, Gareth R. Eaton, and Sandra S. Eaton

Department of Chemistry and Biochemistry, University of Denver, Denver, Colorado 80208

Received September 10, 1999; revised January 26, 2000

The temperature dependence of spin–lattice relaxation rates was analyzed for four high-spin nonheme iron proteins between 5 and 20 K, for three high-spin iron porphyrins between 5 and 118 K, and for four high-spin heme proteins between 5 and 150 to 298 K. For the nonheme proteins the zero-field splittings, D, are less than 0.7 cm^{-1}, and the relaxation is dominated by the Orbach and Raman processes. For the iron porphyrins and heme proteins D is between 4 and 12 cm^{-1} and the relaxation is dominated by the Orbach process between about 5 and 100 K and by a local mode at higher temperatures. The relaxation rates for the heme proteins in glassy matrices extrapolated to values at room temperature that are similar to values obtained by NMR relaxivity in fluid solution. This similarity suggests that for high-spin Fe(III) heme proteins with effective intramolecular spin–lattice relaxation processes, the additional motional freedom gained when a relatively large protein goes from glassy solid to liquid solution at room temperature has little impact on spin–lattice relaxation.

Key Words: **Debye temperature; electron spin–lattice relaxation; high-spin Fe(III); local vibrational mode; methemoglobin; metmyoglobin; Orbach process; Raman process.**

INTRODUCTION

Early studies of electron spin–lattice relaxation for high-spin Fe(III) were performed predominantly at temperatures below about 10 K. The temperature dependence of $1/T_1$ characteristic of the Orbach process has been observed by EPR for high-spin Fe(III) in camphor-bound cytochrome P-450 from *Pseudomonas putida* between 1.5 and 2.5 K ($D = 3.5$ cm^{-1}) (*1*) for whale aquo-metmyoglobin in randomly oriented (*2, 3*) or single crystal (*2*) samples between 2 and 4 K ($D = 9.26$ (*2*) or 7.92 cm^{-1} (*3*)), for aquo-methemoglobin and aquo-metmyoglobin between 4.2 and 10 K ($D = 7.0$ or 7.2 cm^{-1}, respectively) (*4*), and for whale fluoro-metmyoglobin in 1:1 water: glycerol between 2 and 4 K ($D = 6.1$ cm^{-1}) (*2*). The influence of iron spin–lattice relaxation on the hyperfine splitting in Mössbauer spectra of whale aquo-metmyoglobin between 5 and 10 K exhibited the temperature dependence characteristic of an Orbach process (*5, 6*) and above 60 K it was proposed that the Raman process dominated (*6*). The temperature dependence of CW EPR linewidths for aquo-metmyoglobin between 77 and 180 K in water:glycerol was fitted to the Raman process with a Debye temperature of 116 K (*7*). The relaxation of Fe(III) in a single crystal of calcite between 1.4 and 195 K was fitted to a direct process at low temperature and a Raman process with a Debye temperature of 463 K at higher temperature (*8*). These studies demonstrate the dominance of the Orbach process for heme proteins at low temperatures and suggest that the Raman process may be important at higher temperatures in immobilized samples. The Raman and Orbach processes are two-phonon processes, which means that the energy to be released to the lattice is the difference between the energies of two phonon modes. The Orbach process involves a low-lying excited state. The Raman process involves a virtual excited state. In fluid solution, Fe(III) relaxation rates have been estimated from NMR proton relaxivity measurements (*9–14*) and are of interest to design NMR contrast agents.

As part of our studies of the effect of a more rapidly relaxing spin on the relaxation rate of a more slowly relaxing spin to obtain interspin distances (*15, 16*), we seek to understand the temperature dependence of the relaxation rates for high-spin Fe(III) at temperatures between 5 and 300 K. In this report we analyze the temperature dependence of spin–lattice relaxation for four nonheme Fe(III) samples with zero-field splittings (D) less than 0.7 cm^{-1} (1 K) and seven heme Fe(III) samples with D between 4 and 12 cm^{-1} (5.7 and 18 K). For comparison, data are included for one Cr(III) ($S = \frac{3}{2}$) complex.

EXPERIMENTAL METHODS

Horse heart myoglobin (Mb, Sigma) was used without purification. Mutants of sperm whale myoglobin in which valine 66 was replaced by cysteine (Mb–V66C) or lysine 98 was replaced by cysteine (Mb–K98C) (*17*) were expressed in bacteria as described by Springer and Sliger (*18*). A nitroxyl spin label was attached to the cysteines in Mb–V66C and Mb–K98C and the heme iron was oxidized to Fe(III) to prepare *R*–Mb–V66C and *R*–Mb–K98C (*17*). To form the fluoride adducts, 200 mM fluoride was added to solutions at pH 6.8. To prepare the formate adducts (*9*), 3 M sodium formate pH 7.0 in 50% glycerol was added and the sample was concentrated. The addition of formate and subsequent sample concentration was repeated several times. Conversion to high-spin iron was con-

1090-7807/00 $35.00

firmed by CW EPR spectra at 15 K. Tris(oxalato) chromium(III) ($Cr(ox)_3^{3-}$) was prepared by the method of Bailar and Young (*19*). 1:1 v:v glycerol was added to the aqueous samples to ensure glass formation. Sample concentrations after addition of glycerol were 0.3 to 2 mM and in this concentration range the relaxation rates are independent of concentration. Samples were degassed by three to four freeze–pump–thaw cycles. Horse heart Mb–F in sucrose glass was prepared by dissolving 4.5 mg Mb and 0.3 g sucrose in 3 mL of 30 mM phosphate buffer, pH 7.0, containing 200 mM F^- followed by lyophilization overnight. Horse heart Mb–formate in sucrose glass was prepared by dissolving 4.5 mg Mb and 0.3 g sucrose in 3 mL of 1 M sodium formate-formic acid buffer, pH 7.0, followed by lyophilization overnight. The sucrose glasses were placed in EPR tubes that were evacuated overnight to remove residual water and back-filled with a partial pressure of helium.

Spin–lattice relaxation rates, $1/T_1$, for the Fe(III) complexes up to about 10^6 s^{-1} were measured by 3-pulse inversion recovery on a Bruker ESP380E spectrometer. For $Cr(ox)_3^{3-}$ $1/T_1$ was determined by saturation recovery on a locally constructed spectrometer (*20*). Experimental data were fitted to a single exponential using a nonlinear least-squares algorithm. Fits of the data to the sum of two exponentials frequently were better than to a single exponential. However, the temperature dependence was essentially the same for the time constants obtained by the single- and double-exponential fits. Because there is less scatter in the time constants obtained from the single-exponential fits, these values were used in the analysis of the temperature dependence of the relaxation rates. Deviations from a single exponential may be due to a distribution in relaxation rates.

For Mb–F, *R*–Mb–F, Mb–formate, and *R*–Mb–formate the linewidths of the EPR signals in the CW spectra are temperature dependent above about 15 K. In this temperature range the electron spin relaxation time constant T_2 was determined from the temperature-dependent contribution to the linewidth (*15*) and the assumption was made that $T_1 = T_2$. For the iron porphyrins and heme proteins the relaxation rate at ca. 5 K is orientation dependent, but rates at temperatures above about 15 K are not orientation dependent (*15, 16*). The data analyzed in this study were obtained in the perpendicular plane ($g \sim 6$). There is no interference from the spin label signal in this region of the spectrum and the iron relaxation rate was not impacted by the presence of the spin label.

Temperatures between 4.2 and 70 K were obtained with an Oxford 935 cryostat on the ESP380E or an Oxford ESR900 on the saturation recovery spectrometer. Temperatures between 90 and 298 K were obtained with a Varian liquid-nitrogen cooled-gas flow system. The temperature at the sample relative to the Oxford readout was calibrated by replacing the sample with a tube containing a thermocouple immersed in 1:1 H_2O: glycerol. The estimated uncertainty in temperature is about 1 K.

In addition to the data obtained for these samples, previously published data for the temperature dependence of $1/T_1$ for tris(oxalato)ferrate ($Fe(ox)_3^{3-}$) (*21*), iron transferrin carbonate ($FeTfCO_3$) (*21*), iron transferrin oxalate (FeTfoxalate) (*21*), iron enterobactin bound to iron protein *A* (FeEnt) (*22*), iron tetratolylporphyrin fluoride (FeTTPF) (*15*), iron tetratolylporphyrin chloride (FeTTPCl) (*15*), iron tetratolylporphyrin bromide (FeTTPBr) (*15*), methemoglobin fluoride (Hb–F) (*16*), and aquo methemoglobin (Hb–H_2O) (*16*) were analyzed. Uncertainties in T_1 are about 10%.

The experimental data for $1/T_1$ as a function of temperature were fitted to Eq. [1] by minimizing the sum of the residuals on a log–log scale.

$$\frac{1}{T_1} = A_{\mathrm{dir}}T + A_{\mathrm{Ram}}\left(\frac{T}{\theta_{\mathrm{D}}}\right) J_8\left(\frac{\theta_{\mathrm{D}}}{T}\right) + A_{\mathrm{loc}}\left[\frac{e^{\Delta_{\mathrm{loc}}/T}}{(e^{\Delta_{\mathrm{loc}}/T}-1)^2}\right] + A_{\mathrm{Orb}}\left[\frac{\Delta_{\mathrm{Orb}}^3}{e^{\Delta_{\mathrm{Orb}}/T}-1}\right] + A_{\mathrm{Orb2}}\left[\frac{\Delta_{\mathrm{Orb2}}^3}{e^{\Delta_{\mathrm{Orb2}}/T}-1}\right], \qquad [1]$$

where T is temperature in Kelvins, A_{dir} is the coefficient for the contribution from the direct process, A_{Ram} is the coefficient for the contribution from the Raman process, θ_{D} is the Debye temperature, J_8 is the transport integral,

$$J_8\left(\frac{\theta_{\mathrm{D}}}{T}\right) = \int_0^{\theta_{\mathrm{D}}/T} x^8 \frac{e^x}{(e^x-1)^2}\,dx,$$

A_{loc} is the coefficient for the contribution from a local vibrational mode, Δ_{loc} is the energy for the local mode in Kelvins, A_{Orb} and A_{Orb2} are the coefficients for the contribution from the Orbach process involving the two excited Kramers' doublets at 2D and 6D, and Δ_{Orb} and Δ_{Orb2} are the energy separations between the ground state and the two excited states for the Orbach process in Kelvins.

Mathematical expressions for the temperature dependence of spin–lattice relaxation are taken from the following references: Raman process (*23, 24*), local mode (*25*), and Orbach process (*26*). Equation [1] includes the Orbach process for the middle Kramers' doublet ($\Delta_{\mathrm{Orb}} = 2\mathrm{D}$) and the upper Kramers' doublet ($\Delta_{\mathrm{Orb2}} = 6\mathrm{D}$) of the high-spin heme. For each process the full mathematical form of the expression was used to permit application over a wide range of temperatures.

Strategy Used in Fitting the Experimental Data

The temperature dependence of $1/T_1$ for the Raman process is distinctive if data are available over a sufficiently wide temperature range and if the Raman process dominates. The Raman process has been observed to dominate spin–lattice relaxation for organic radicals in dilute glassy solutions between about 10 and 100 K (*27*). The direct process results in a linear dependence of $1/T_1$ on temperature and has been ob-

TABLE 1
Relaxation Processes for High-Spin Complexes[a]

Sample	Lattice	Temperature range (K)	Orbach, A_{Orb}, A_{Orb2}, $2D$	Raman, A_R, θ_D	Local, A_{loc}, Δ_{loc}
$Cr(ox)_3^{3-}$	H_2O:glyc	15–70	3.6×10^{2}[b], 2.0	1.2×10^{7}, 85	1.0×10^{7}[b], 300
$Fe(ox)_3^{3-}$	H_2O:glyc	7–30	1.4×10^{3}, 1.4×10^{3}[c], 0.43	4.7×10^{7}, 65	
FeTfoxalate	H_2O:glyc	5–20	1.0×10^{3}, 1.0×10^{3}[c], 0.70	1.6×10^{7}, 52	
$FeTfCO_3$	H_2O:glyc	5–20	7.6×10^{2}, 7.6×10^{2}[c], 0.86	2.7×10^{7}, 52	
FeEnt	H_2O:glyc	6–20	3.4×10^{2}, 3.4×10^{2}[c], 1.4	2.3×10^{7}, 52	
FeTTPF	toluene	4.5–118	2.0×10^{3}, 1.7×10^{4}, 11		
FeTTPCl	toluene	4.6–117	1.5×10^{4}, 1.4×10^{4}, 18		
FeTTPBr	toluene	4.5–118	9.4×10^{4}, 1.0×10^{2}, 32		
Mb–F	H_2O:glyc	4.8–298	1.9×10^{3}, 1.9×10^{3}, 14		4.5×10^{9}[b], 1000
Mb–F[d]	H_2O:glyc	2–4	6.1×10^{3}, na, 17.5		
Hb–F	H_2O:glyc	4.2–150	2.4×10^{3}, 5.8×10^{2}, 17		2.7×10^{9}[b], 300
Mb–formate	H_2O:glyc	4.6–298	6.4×10^{3}, 1.1×10^{3}, 23		2.9×10^{10}[b], 700
Mb–H_2O[d]	H_2O:glyc	2–4	9.9×10^{3}, na, 26.3		
Hb–H_2O	H_2O:glyc	4.3–150	2.0×10^{4}, 3.9×10^{3}, 30		

[a] Energies ($2D$, θ_D, Δ_{loc}) are in Kelvin.
[b] Process makes small contribution in temperature range examined so parameters are very uncertain.
[c] A_{Orb} was set equal to A_{Orb2} in the fitting procedure.
[d] To be consistent with the form of Eq. [1], values of the coefficient A_{Orb} reported in units of s^{-1} by Scholes *et al. Biochim. Biophys. Acta* **244,** 206–210 (1971) were converted to s^{-1} K^{-3} by dividing by $(2D)^3$.

served to dominate at low temperature for a variety of metal ions (*28*). An approximately linear dependence on T also is observed in the high-temperature limit of the Orbach process (*26*) and in the high-temperature limit for a local vibrational mode that can be approximated as a tunneling oscillator (*24*). Similar ambiguities in assigning relaxation processes arise because the temperature dependence of $1/T_1$ is essentially the same for the Orbach process and for a local mode when the temperatures are less than the characteristic energy, Δ_{Orb} or Δ_{loc}. Thus when data are available over a limited temperature range, distinctions between some processes require judgments concerning plausibility of a process for a particular paramagnetic center.

Since zero-field splittings of the magnitude observed for many high-spin Fe(III) complexes provide low-lying excited states, the Orbach process is a plausible relaxation process for Fe(III) complexes. Literature values of D are: $Fe(ox)_3^{3-}$, 0.09 to 0.20 cm^{-1} (0.13 to 0.28 K) depending upon the lattice (*29*); $FeTfCO_3$ and FeTfoxalate, 0.25–0.27 cm^{-1} (0.36–0.39 K) (*30, 31*); FeEnt, 0.50 cm^{-1} (0.71 K) (*32*); FeTPPF, ~4 cm^{-1} (~5.7 K) (*15*); FeTPPCl, 6.0 to 8.0 cm^{-1} (8.6–11.4 K) (*33–37*); FeTPPBr, 12.5 cm^{-1} (17.9 K) (*38*); Mb–F and Hb–F, 5.9 to 6.5 cm^{-1} (8.4 to 9.3 K) (*2, 39–42*); Mb–H_2O and Hb–H_2O, ~8 to 11 cm^{-1} (11.4 to 15.7 K) (*2, 3, 16*); and $Cr(ox)_3^{3-}$, 0.68 to 0.78 cm^{-1} (0.97 to 1.1 K) (*43–45*).

For each sample, the temperature dependence of $1/T_1$ was fitted with the smallest number of contributing processes consistent with the experimental data. The resulting best-fit parameters are given in Table 1. In the least-square procedure D was held within ±20% of median literature values. Changing A_{Orb} or A_{Orb2} by 10–20%, without compensating changes in other parameters, caused a significant increase in the standard deviation for the fitted line. Errors in the coefficients A_{Orb} and A_{Orb2} are correlated with errors in D because increasing the characteristic energy requires increasing the coefficient to obtain approximately the same relaxation rate at a particular temperature. Although the overall fit function is dependent on both A_{Orb} and A_{Orb2}, the fit at lower temperatures is more sensitive to A_{Orb} than to A_{Orb2}. Uncertainties in the temperature calibrations at the lower temperatures could cause systematic errors in A_{Orb} that can be partially compensated by changes in A_{Orb2}. The values of A_{Ram} and θ_D obtained for the samples with small D are quite uncertain because of the overlap with the Orbach process. For the samples in which a local mode was invoked, its contribution was significant over a relatively narrow range of temperatures well below Δ_{loc}, which makes the fit parameters quite uncertain. Thus the numerical values of some of the fit parameters are quite uncertain, despite the fact that the overall shapes of the plots of $\log(1/T_1)$ vs $\log(T)$ clearly require contributions from several types of relaxation processes.

RESULTS

The slopes of plots of $\log(1/T_1)$ vs $\log(T)$ for $Cr(ox)_3^{3-}$ and FeEnt are approximately 2 (Fig. 1). Thus, $1/T_1$ varies approximately as T^2. A similar temperature dependence of $\log(1/T_1)$ was observed for $Fe(ox)_3^{3-}$, FeTfoxalate, and $FeTfCO_3$, which also have D less than about 1 K. This is the temperature dependence expected in the high temperature limit for the

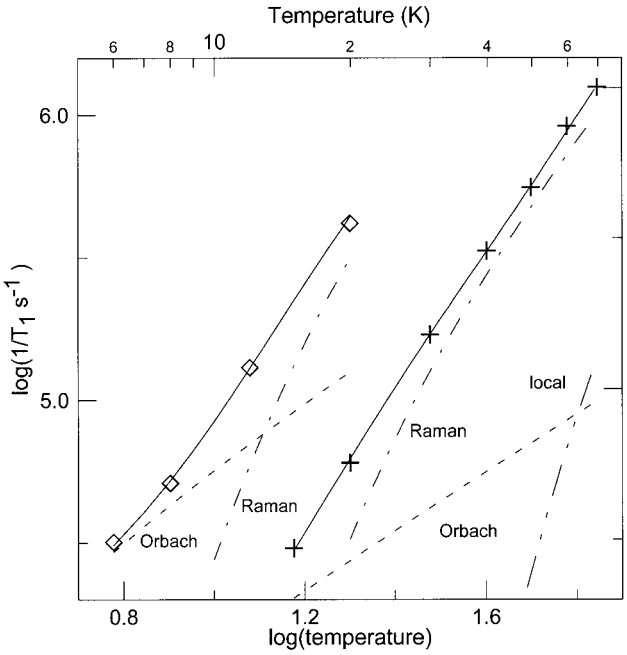

FIG. 1. Temperature dependence of *X*-band spin–lattice relaxation rates for 1.0 mM $Cr(ox)_3^{3-}$ in 1:1 water:glycerol (+) measured at the $g_\perp$ turning point and for 0.2 mM FeEnt in 1:1 water:glycerol (◇) (*22*). The solid lines through the data are the fits obtained using Eq. [1] and the parameters in Table 1. The individual contributions are: (– –) Orbach process involving excited states at 2*D* and 6*D*, (– - –) Raman process, and (– - - –) local mode.

Raman process. The onset of limiting behavior occurs at a smaller fraction of θ_D in glasses than in crystalline solids because of the greater role of low frequency vibrations in glasses (*46, 47*) than in crystals; however, it is still not plausible that the Debye temperature is low enough to be in the high temperature limit at 10 K. The temperature dependence of the relaxation rates for these five samples could not be fit with the Raman process alone and required a contribution from another process that makes a significant contribution at lower temperatures. That process could be modeled either as the direct process or as an Orbach process. Since the zero-field splitting provides low-lying excited states, an Orbach process was selected to give the fits shown in Fig. 1 and the parameters shown in Table 1. Since all of the relaxation rate data for these complexes were obtained at temperatures much larger than *D*, the data are in the high-temperature limit for the Orbach process, and it is not possible to distinguish between the contributions from the excited states at 2*D* and 6*D*. Therefore, the coefficients for these two contributions were assumed to be equal. Comparable agreement between experimental and calculated temperature dependence of $1/T_1$ could be obtained by using the direct process instead of the Orbach process as the low-temperature contribution. For $Cr(ox)_3^{3-}$ a small additional contribution at higher temperatures was modeled as a local mode.

The temperature dependence of $1/T_1$ for FeTTPX (Fig. 2) is substantially different from that observed for the non-heme iron samples. Above 20 to 30 K the slopes of the plots of $\log(1/T_1)$ vs $\log(T)$ for FeTTPX are about 1, as expected for the high-temperature limit of the Orbach process. The upper temperature for the measurements on these samples (118 K) was limited by the softening temperature (~120 K) of the toluene glass (*48*). It is assumed that *D* for FeTTP*X*, *X* = F, Cl, Br, is approximately the same as for the analogous TPP complex and thus is in the range of 4 to 12.5 cm^{-1} (*15, 33–38*). Over the temperature interval for which data were available, the temperature dependence of $1/T_1$ for FeTTP*X* could be fitted using only the Orbach process with excited states at 2*D* and 6*D* (Table 1).

For Hb–F up to about 100 K, and for Hb–aquo, the temperature dependence of $1/T_1$ (Fig. 3) is similar to that observed for the iron(III) porphyrins (Fig. 2). Data for Hb–F and Hb–aquo extend to higher temperatures than for the iron porphyrins because the glass softening temperature is higher for 1:1 water: glycerol than for toluene. The simulated curves for Hb–F and Hb–aquo (Fig. 3) are dominated by the Orbach process with excited states at 2*D* and 6*D* (Table 1). For Hb–F, an additional process, which was modeled as a local mode, makes a substantial contribution above about 100 K.

Figure 4 includes values of $1/T_1$ in the perpendicular plane ($g \sim 6$) for Mb–F, *R*–Mb–F, Mb–formate, and *R*–Mb–formate in 1:1 water:glycerol and for Mb–F and Mb–formate in sucrose

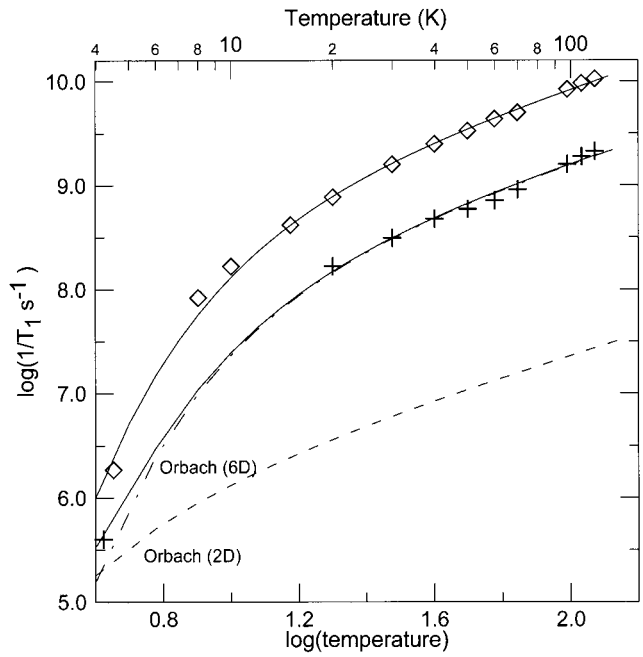

FIG. 2. Temperature dependence of *X*-band spin–lattice relaxation rates for the $m_s = \pm\frac{1}{2}$ transitions for 1.0 mM FeTTPF (+) and for FeTTPBr (◇) in toluene (*15*). The solid lines through the data are the fits obtained using Eq. [1] and the parameters in Table 1. The individual contributions to the relaxation for FeTTPF are: (– –) Orbach process involving excited state at 2*D* and (– - –) Orbach process involving excited state at 6*D*.

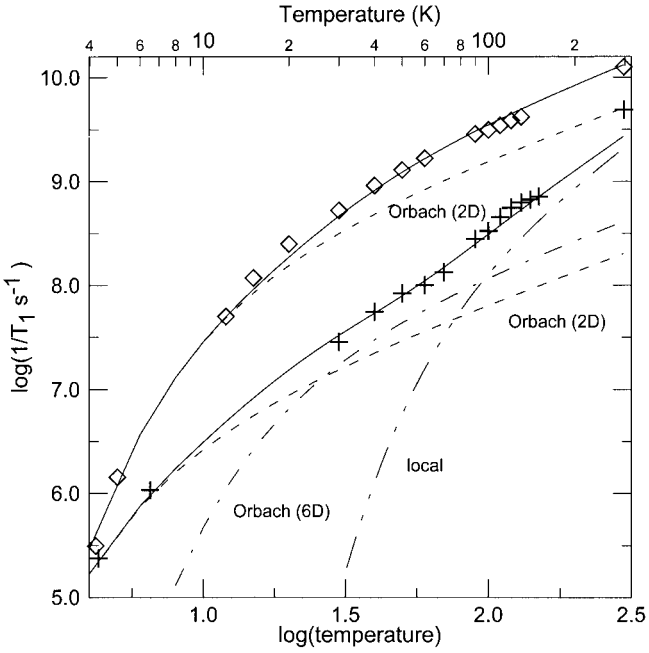

FIG. 3. Temperature dependence of *X*-band spin–lattice relaxation rates for the $m_s = \pm\frac{1}{2}$ transitions for Hb–F (+) and for Hb–H_2O (◇) in 1:1 water:glycerol (*16*). The solid lines through the data are the fits obtained using Eq. [1] and the parameters in Table 1. The individual contributions to the relaxation are: (– –) Orbach process involving excited state at 2*D*, (– - –) Orbach process involving excited state at 6*D*, and (– - - –) local mode. The data points at 298 K are values of T_{1e} obtained by analysis of NMR spin–lattice relaxation rates for water protons in solutions of Hb–F or Hb–aquo (*9–14*).

glass. Within experimental uncertainty, relaxation rates for the Fe(III) in the spin-labeled sperm whale variants were the same as in the wild-type horse heart myoglobin at the same temperature so data were combined. Between about 100 and 160 K iron relaxation rates for horse heart Mb–F and Mb–formate were obtained in both 1:1 water:glycerol and in the sucrose glass and comparisons indicate that there is not a significant difference between the values of $1/T_1$ obtained in the two hosts. The shapes of the curves in Fig. 4 indicate that the relaxation rates between about 5 and 100 K are dominated by the Orbach process. The linewidth of the CW EPR signal for Mb–formate in room temperature solution is slightly narrower than the signal for Mb–aquo (*49*). We therefore assumed that the ZFS for Mb–formate is somewhat smaller than for Mb–aquo ($D \sim 9.5$ cm^{-1}) and $D = 8$ cm^{-1} ($2D = 23$ K) was used in the simulations of the spin–lattice relaxation data for Mb–formate. The shapes of the plots in Fig. 4 indicate that an additional process makes a substantial contribution to the relaxation above about 100 K for Mb–formate and above about 200 K for Mb–F, and these processes were modeled as local modes.

DISCUSSION

The temperature dependence of the spin–lattice relaxation rates, $1/T_1$, is substantially different for $Cr(ox)_3^{3-}$ and nonheme iron(III) samples with *D* less than about 1 cm^{-1} (Fig. 1) than for the heme iron(III) samples with *D* substantially greater than 1 cm^{-1} (Figs. 2–4). For $Cr(ox)_3^{3-}$ (Fig. 1) the temperature dependence of the relaxation was fitted with an Orbach process that dominated below about 20 K, the Raman process that dominated between about 30 and 60 K, and increasing contributions from a local mode above about 60 K. The relaxation rates for Cr^{3+} in a crystal of MgO are about three orders of magnitude slower than for $Cr(ox)_3^{3-}$ and the temperature dependence of $1/T_1$ was fitted to a sum of the direct process, the Raman process, and a local vibrational mode with an energy of 537 K (*50*), although a contribution from an Orbach process does not appear to have been considered. For Cr^{3+} in MgO the Raman process dominated between about 30 and 40 K. Thus, except for the assignment of the lowest temperature process as direct rather than Orbach, the relaxation processes for Cr^{3+} in MgO are similar to those for $Cr(ox)_3^{3-}$. The slower relaxation rates for Cr^{3+} in MgO than for $Cr(ox)_3^{3-}$ probably are the result of the much smaller zero-field splitting in the high-symmetry cubic site of MgO than in the lower symmetry oxalate complex.

For the nonheme Fe(III) samples with small zero-field splittings, the Raman process dominates the relaxation above about 15 K. The Debye temperatures obtained for $Cr(ox)_3^{3-}$ and $Fe(ox)_3^{3-}$ are 85 and 65 K, which are smaller than observed in

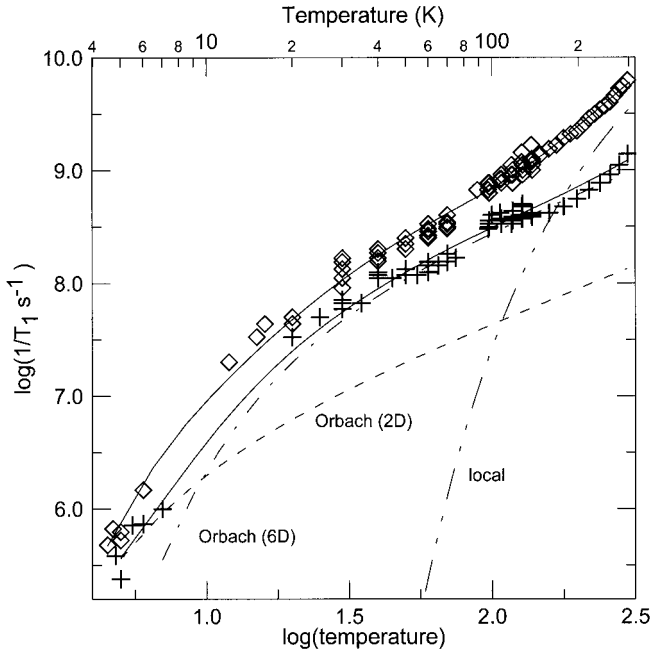

FIG. 4. Temperature dependence of *X*-band spin–lattice relaxation rates for the $m_s = \pm\frac{1}{2}$ transitions for Mb–F and *R*–Mb–F (+) and for Mb–formate and *R*–Mb–formate (◇) in 1:1 water:glycerol and in a sucrose glass. The solid lines through the data are the fits obtained using Eq. [1] and the parameters in Table 1. The individual contributions to the relaxation for Mb–F and *R*–Mb–F are: (– –) Orbach process involving excited state at 2*D* and (– - –) Orbach process involving excited state at 6*D*. The contribution to the relaxation of Mb–formate and *R*–Mb–formate from a local mode (– - - –) also is shown.

1:1 water:glycerol for small organic radicals and transition metal complexes with $S = \frac{1}{2}$ (θ_D = 112 to 120 K) (*27*). Similarly, the Debye temperatures obtained for FeTfoxalate, $FeTfCO_3$, and FeEnt (52 K) are smaller than observed for low-spin hemes (θ_D = 78 to 80 K) (*27*). The small temperature interval over which data were obtained for the nonheme Fe(III) samples and the overlap with the Orbach process may cause significant uncertainty in the values of the Debye temperature. Data were not obtained at high enough temperatures to evaluate the possible contributions of local modes to the relaxation rates for the nonheme iron.

For the iron porphyrins and heme proteins (Figs. 2–4) the relaxation rates between 5 and about 100 K were dominated by the Orbach process. If the coefficients for the Raman process for the iron porphyrins and heme proteins were similar to those observed for the nonheme proteins, the contribution of the Raman process to the relaxation rates for the porphyrin and heme samples would be negligible compared to the Orbach process. At higher temperatures an additional process was observed for Hb–F, Mb–formate, and Mb–F that was modeled as a local mode. The characteristic energies for these local modes are very uncertain because the contributions from these processes were relatively small in the temperature range over which experimental data were obtained, and the highest temperature at which data were obtained is well below Δ_{loc}.

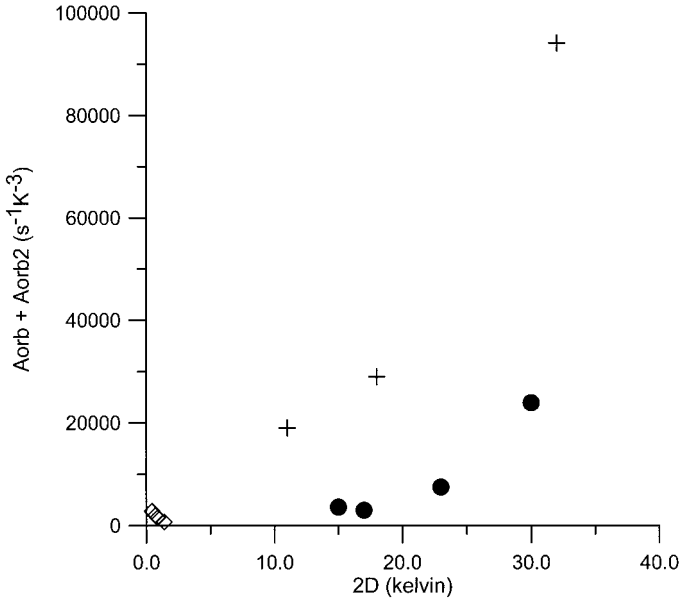

FIG. 5. Dependence of the combined coefficients of the Orbach process ($A_{orb} + A_{orb2}$) obtained by fitting the temperature dependence of $1/T_1$, on the zero-field splitting, $2D$, for the series of Fe(III) compounds: nonheme iron with small zero-field splittings (◇), iron porphyrins (+), and heme proteins (●).

Coefficients of the Orbach Contribution

The coefficients of the Orbach contributions are summarized in Table 1. The values of A_{Orb}, the coefficient for the process involving the excited state at $2D$, obtained from fitting data for Mb–F and Hb–F between 5 and 298 or 150 K are within a factor of 3 of those obtained previously for Mb–F between 2 and 4 K (*2*) and the value for Hb–H_2O is within a factor of 2 of that reported for Mb–H_2O (*2*) (Table 1). The agreement between coefficients obtained in such different temperature intervals supports the assertion that the Orbach relaxation process dominates over a wide temperature interval for the heme proteins. There is not a clear pattern in the relative values of the coefficients for the Orbach contributions from the excited states at $2D$ and $6D$. So, to qualitatively examine trends in the effectiveness of the Orbach process in inducing spin–lattice relaxation, the sum of $A_{Orb} + A_{Orb2}$ is plotted as a function of $2D$ in Fig. 5. Within the set of iron porphyrins, FeTPP*X*, the sum of the coefficients increases as $2D$ increases, as expected if modulation of the zero-field splitting dominates the relaxation. Similarly, within the series of heme proteins there is a general trend toward larger coefficients as $2D$ increases. However, for comparable values of $2D$ the coefficients for the heme proteins are much smaller than for the iron porphyrins (Table 1, Fig. 5). Modulation of the zero-field splitting by motion of the axial ligands is likely to be a significant contribution to the relaxation. In the heme proteins, the axial ligands are hydrogen bonded (*51, 52*) to water molecules or protein side chains, which substantially restricts the motional freedom of the ligands compared with that in the small molecules, which may account for the smaller coefficients, A_{Orb} and A_{Orb2}. Similarly, in studies of $S = \frac{1}{2}$ complexes it was observed that the coefficients of the Raman process were larger for more flexible molecules than for rigid molecules (*27, 53*). We propose that molecular flexibility is a significant factor in the coefficients for both the Raman and Orbach processes.

Relaxation Rates at Room Temperature

The relaxation rates for high-spin Fe(III) in fluid solution at room temperature have been calculated from the effects of the rapidly relaxing iron on the relaxation rate for water protons measured by NMR. The calculated values are model dependent so there is a substantial spread in the resulting values. Within the uncertainty of those values there does not appear to be a difference between hemoglobin and myoglobin so we group the values by axial ligand rather than by protein. For Hb–F and Mb–F the calculated values of the electron spin relaxation time constant, T_1, at room temperature range from 3.5×10^{-11} to 9×10^{-10} s with a median value of about 2×10^{-10} s (*9–13*) and for Hb–H_2O and Mb–H_2O the values range from 4.4×10^{-11} to 2.8×10^{-10} with a median value of about 8×10^{-11} s (*10–12, 14*). The median values are included in Fig. 3, which shows that extrapolation of the data for Hb–F and Hb–aquo in glassy 1:1 water:glycerol gives values in reasonable agreement with the fluid solution data, particularly when the uncertainty in the fluid solution values is taken into account. Extrapolation

of the fitted curve for Mb–formate in glassy 1:1 water:glycerol and in glassy sucrose gives $T_1 = 1.6 \times 10^{-10}$ s at 298 K. The somewhat longer extrapolated value for Mb–formate than calculated from NMR relaxivity for Mb–H_2O and Hb–H_2O in solution is in the direction expected if D is somewhat smaller for Mb–formate than for Mb–H_2O. The T_1 values obtained from the EPR linewidths are for the $m_s = \pm\frac{1}{2}$ transition. The NMR values are averages for all m_s values. Transitions involving $m_s = \pm\frac{3}{2}$ and $m_s = \pm\frac{5}{2}$ may have shorter T_1 than for $m_s = \pm\frac{1}{2}$ (*54*), which also would make the values of T_1 determined by NMR shorter than the values calculated from the EPR linewidths. For these large molecules with relatively efficient processes for electron spin relaxation it appears that the additional motional freedom that is gained by going from the glassy solid to fluid solution at room temperature has little impact on the spin–lattice relaxation. For Mb–F, the value of T_1 in the sucrose glass at 298 K is 7.2×10^{-10} s, which is about a factor of 3.5 longer than the median value in fluid solution. In glassy sucrose, Mb–F has the longest T_1 of the hemes studied. When T_1 in the glassy phase is this long near 298 K, the additional motion that occurs in fluid solution may make a more significant contribution to the relaxation than is observed for hemes that relax more quickly in the glassy state.

In aqueous solution the dependence of the EPR linewidths for $Fe(H_2O)_6^{3+}$ and related lower symmetry small-molecule complexes on temperature, viscosity, and external magnetic field strength were examined (*55, 56*). It was concluded that T_2 is determined by collisions with solvent molecules that modulate the zero-field splitting with correlation times of about 5×10^{-12} s (*55, 56*). These collisions also may dominate T_1 for small Fe(III) complexes in fluid solution (*57*). The modulation of the zero-field splitting for a metal bound inside a protein is likely to be dominated by motions of protein side chains rather than solvent molecules. Even in the "solid" or glassy state, there is substantial motion of atoms in proteins (*58*), exceeding that expected solely for vibrations (*59*). A further indication of the motional freedom of atoms in solid samples of proteins is an optical spectroscopy study of myoglobin which found that the protein was glass-like below 180 K and liquid-like at higher temperatures (*60, 61*). Thus, it seems plausible, that in a metalloprotein, the motions that modulate the zero-field splitting and cause spin–lattice relaxation may not change substantially on going from a glassy solid to fluid solution. If the spin–lattice relaxation is dominated by motion of protein atoms, changes in the environment surrounding the protein may have little effect on spin–lattice relaxation.

Comparison with Low-Spin Hemes

For low-spin heme the temperature dependence of T_1 at X-band between about 5 and 100 K was modeled with a small contribution from the direct process, the Raman process, and either a local mode or a thermally activated process with a characteristic energy of about 175 cm^{-1} (*27*). The relaxation is attributed to modulation of spin–orbit coupling. For metmyoglobin the spin–lattice relaxation rates are faster for high-spin than for low-spin Fe(III) below 40–50 K, but rates are faster for low-spin than for high-spin at higher temperatures.

ACKNOWLEDGMENTS

The support of this work by National Institutes of Health GM21156 (GRE and SSE) and GM57635 (BEB) is gratefully acknowledged.

REFERENCES

1. R. C. Herrick and H. J. Stapleton, *J. Chem. Phys.* **65,** 4786–4790 (1976).
2. C. P. Scholes, R. A. Isaacson, and G. Feher, *Biochim. Biophys. Acta* **244,** 206–210 (1971).
3. P. D. Levin and A. S. Brill, *J. Phys. Chem.* **92,** 5103–5100 (1988).
4. E. Wajnberg, H. J. Kalinoski, G. Bemski, and J. S. Helman, *Biophys. J.* **49,** 1195–1198 (1986).
5. A. M. Afanas'ev, E. Yu. Tsymbal, V. M. Cherepanov, S. S. Yakimov, and F. Parak, *Sov. Phys. JETP* **65,** 1246–1251 (1987). Note that the analysis of the Mössbauer data extracts rates for transitions between energy levels with separations on the order of the zero-field splitting. The expressions for the temperature dependence of the rates are different than those for the temperature dependence of $1/T_1$ for the same process.
6. A. R. Bizarri, O. A. Iakovleva, and F. Parak, *Chem. Phys.* **191,** 185–194 (1995).
7. A. R. Bizarri and S. Cannistraro, *Appl. Magn. Reson.* **6,** 575–586 (1994).
8. S. A. Marshall, S. V. Nistor, and R. A. Serway, *Phys. Rev. B* **6,** 1686–1689 (1972).
9. S. Aime, M. Fasano, S. Paoletti, F. Cutruzzola, A. Desideri, M. Bolognesi, M. Rizzi, and P. Ascenzi, *Biophys. J.* **70,** 482–488 (1996).
10. T. Asakura, G. H. Reed, and J. S. Leigh, Jr., *Biochemistry* **11,** 334–338 (1972).
11. M. E. Fabry and M. Einsenstadt, *J. Biol. Chem.* **249,** 2915–2929 (1974).
12. R. K. Gupta and A. S. Mildvan, *J. Biol. Chem.* **250,** 246–253 (1975).
13. S. H. Koenig, R. D. Brown, III, and T. R. Lindstrom, *Biophys. J.* **34,** 397–498 (1981).
14. A. Lanir, *Biochem. Biophys. Acta* **497,** 29–34 (1977).
15. M. H. Rakowsky, A. Zecevic, G. R. Eaton, and S. S. Eaton, *J. Magn. Reson.* **131,** 97–110 (1998).
16. M. Seiter, V. Budker, J.-L. Du, G. R. Eaton, and S. S. Eaton, *Inorg. Chim. Acta* **273,** 354–366 (1998).
17. Y. Zhou, B. E. Bowler, G. R. Eaton, and S. S. Eaton, submitted for publication.
18. B. A. Springer and S. G. Sliger, *Proc. Natl. Acad. Sci. USA* **84,** 8961–8965 (1987).
19. J. C. Bailar, Jr. and E. M. Young, *Inorg. Synth.* **1,** 35 (1939).
20. R. W. Quine, S. S. Eaton, and G. R. Eaton, *Rev. Sci. Instrum.* **63,** 4251–4262 (1992).
21. B. J. Gaffney, G. R. Eaton, and S. S. Eaton, *J. Phys. Chem. B* **102,** 5536–5541 (1998).
22. C. S. Klug, S. S. Eaton, G. R. Eaton, and J. B. Feix, *Biochemistry* **37,** 9016–9023 (1998).

23. A. Abragam, "The Principles of Nuclear Magnetism," pp. 405–409, Oxford University Press, London (1961).

24. J. Murphy, *Phys. Rev.* **145,** 241–247 (1966).

25. J. G. Castle, Jr. and D. W. Feldman, *Phys. Rev. A* **137,** 671–673 (1965).

26. R. Orbach, *Proc. Phys. Soc. (Lond.)* **77,** 821–826 (1961).

27. Y. Zhou, B. E. Bowler, G. R. Eaton, and S. S. Eaton, *J. Magn. Reson.* **139,** 165–174 (1999).

28. K. J. Standley and R. A. Vaughan, "Electron Spin Relaxation Phenomena in Solids," Appendix 2, Plenum Press, New York (1969).

29. D. Collison and A. K. Powell, *Inorg. Chem.* **29,** 4735–4746 (1990).

30. J. Dubach, B. J. Gaffney, K. More, G. R. Eaton, and S. S. Eaton, *Biophys. J.* **59,** 1091–1100 (1991).

31. S. A. Kretchmar, M. Texeira, B.-H. Huynh, and K. N. Raymond, *Biol. Met.* **1,** 26–32 (1988).

32. K. Spartalian, W. T. Oosterhuis, and J. B. Neiland, *J. Chem. Phys.* **62,** 3538–3543 (1975).

33. H. Uenoyama, *Biochem. Biophys. Acta* **230,** 479–481 (1971).

34. D. Dolphin, J. R. Sams, T. B. Tsin, and K. L. Wong, *J. Am. Chem. Soc.* **100,** 1711–1718 (1978).

35. D. V. Behere and S. Mitra, *Inorg. Chem.* **18,** 1723–1724 (1979).

36. D. V. Behere and S. Mitra, *Ind. J. Chem. A* **19,** 505–507 (1980).

37. W. R. Browett, A. F. Fucaloro, T. V. Morgan, and P. J. Stephens, *J. Am. Chem. Soc.* **105,** 1868–1872 (1983).

38. D. V. Behere, R. Birdy, and S. Mitra, *Inorg. Chem.* **20,** 2786–2789 (1981).

39. Y.-C. Fann, J.-L. Ong, J. M. Nocek, and B. M. Hoffman, *J. Am. Chem. Soc.* **117,** 6109–6116 (1995).

40. G. C. Brackett, P. L. Richards, and W. S. Caughey, *J. Chem. Phys.* **54,** 4383–4401 (1971).

41. H. Uenoyama, T. Iizuka, H. Morimoto, and M. Kotani, *Biochim. Biophys. Acta* **160,** 159–166 (1968).

42. M. B. Yim, L. C. Kuo, and M. W. Makinen, *J. Magn. Reson.* **46,** 247–256 (1982).

43. R. A. Bernheim and E. F. Reichenbecher, *J. Chem. Phys.* **51,** 996–1001 (1969).

44. Y. Kawasaki and L. S. Forster, *J. Chem. Phys.* **50,** 1010–1013 (1969).

45. S. Lahiry and R. Kakkar, *Chem. Phys. Lett.* **88,** 499–502 (1982).

46. D. L. Huber, *J. Non-Cryst Solids* **51,** 241–244 (1982).

47. D. L. Huber, *J. Luminescence* **36,** 327–329 (1987).

48. The softening temperature was defined operationally as the temperature above which the EPR spectra of small molecules exhibit significant motional averaging of *g* and *A* anisotropy.

49. R. D. Hershberg and B. Chance, *Biochemistry* **14,** 3885–3891 (1975).

50. R. L. Hartman, J. S. Bennett, and J. G. Castle, Jr., *Phys. Rev. B* **1,** 1946–1953 (1970).

51. J. F. Deatherage, R. S. Loe, and K. Moffat, *J. Mol. Biol.* **104,** 723–728 (1976).

52. E. Leci, A. Brancaccio, F. Cutruzzola, C. T. Allocatelli, C. Tarricone, M. Bolognesi, A. Desideri, and P. Ascenzi, *FEBS Lett.* **357,** 227–229 (1995).

53. J. M. Burchfield, J.-L. Du, K. M. More, S. S. Eaton, and G. R. Eaton, *Inorg. Chim. Acta* **263,** 23–33 (1997).

54. M. Rubenstein, A. Baram, and Z. Luz, *Mol. Phys.* **20,** 67–80 (1971).

55. H. Levanon, G. Stein, and Z. Luz, *J. Chem. Phys.* **53,** 876–887 (1970).

56. H. Levanon, S. Charbinsky, and Z. Luz, *J. Chem. Phys.* **53,** 3056–3064 (1970).

57. I. Bertini and C. Luchinat, *Coord. Chem. Rev.* **150,** 77–110 (1996).

58. M. R. Chance, *Meth. Enzymol.* **226,** 97–118 (1993).

59. H. Frauenfelder and B. McMahon, *Proc. Natl. Acad. Sci. (U.S.)* **95,** 4795–4797 (1998) and references therein.

60. J. S. Ahn, T. Kitagawa, Y. Kanematsu, Y. Nishikawa, and T. Kushida, *J. Luminescence* **64,** 81–86 (1995).

61. Y. Shibata, A. Kurta, and T. Kushida, *J. Luminescence* **66/67,** 13–18 (1996).